ACS APPLIED ELECTRONIC MATERIALS

Article

Cite This: ACS Appl. Electron. Mater. 2020, 2, 147−154

pubs.acs.org/acsaelm

Defect-Assisted High Photoconductive UV−Visible Gain in Perovskite-Decorated Graphene Transistors

Nathan D Cottam,[†] Chengxi Zhang,[†,‡] Lyudmila Turyanska,[*,†,§] Laurence Eaves,[†] Zakhar Kudrynskyi,[†] Evgenii E. Vdovin,[†,∥] Amalia Patanè,[†] and Oleg Makarovsky[†]

[†]School of Physics and Astronomy, University of Nottingham, Nottingham, NG72RD, U.K.

[‡]Key Laboratory of Advanced Display and System Applications, Education of Ministry, Shanghai University, 149 Yanchang Road, Shanghai, 200072, China

[§]Faculty of Engineering, University of Nottingham, Nottingham, NG72RD, U.K.

[∥]Institute for Problems of Microelectronics Technologies, Russian Academy of Sciences, Chernogolovka, 142432, Russia

Supporting Information

ABSTRACT: Recent progress in the synthesis of high stability inorganic perovskite nanocrystals (NCs) has led to their increasing use in broadband photodetectors. These NCs are of particular interest for the UV range as they have the potential to extend the wavelength range of photodetectors based on traditional materials. Here we demonstrate a defect-assisted high photoconductive gain in graphene transistors decorated with all-inorganic cesium lead halide perovskite NCs. The photoconductive gain in the UV−vis wavelength range arises from the charge transfer between the NCs and graphene and enables observation of high photoconductive gain of 10^6 A/W. This is accompanied by a giant hysteresis of the graphene resistance that is strongly dependent on electrostatic gating and temperature. Our data are well described by a phenomenological macroscopic model of the charge transfer from bound states in the NCs into the graphene layer, providing a useful tool for the design of high-photoresponsivity perovskite/graphene transistors.

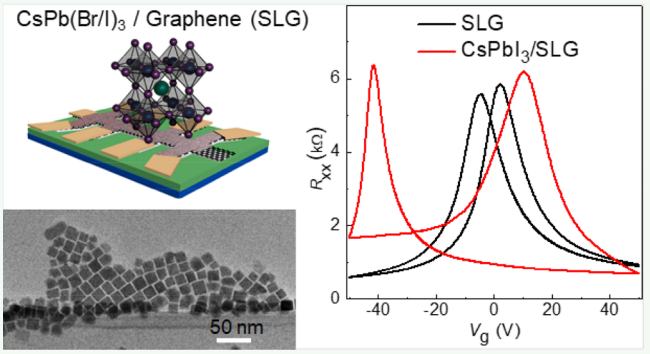

KEYWORDS: *graphene, UV photodetectors, inorganic perovskite nanocrystals, charge transfer, defect levels*

INTRODUCTION

Rapid progress in semiconductor science and technology has led to the development of novel device concepts which combine two-dimensional (2D) van der Waals (vdW) crystals, such as graphene, with an adjacent layer of an optically active 0D, 2D, or 3D material.[1−4] For example, a record high photoresponsivity ($R > 10^9$ A/W) has been achieved by depositing photoresponsive 0D nanocrystals (NCs) of II−VI or IV−VI QDs (CdSe, CdS, PbS, etc.) on the surface of single layer graphene (SLG).[4−6] These hybrid structures are of particular interest for near-infrared (NIR) graphene-based complementary metal-oxide-semiconductor (CMOS) image sensors.[7] More recently, organic[8] and inorganic[9] perovskite nanocrystals with high optical quantum yield have been used in combination with graphene[10−13] to achieve photoresponsivity of up to 10^9 A/W and detectivity of 10^9 Jones. These NCs were also proposed for extending the photoresponsivity of graphene devices to the UV region.[9,10]

Harnessing the potential of the perovskite NC/graphene hybrid materials requires a fundamental understanding of the charge transfer processes that occur at their interface. It is well-known that the electrical properties of graphene are extremely sensitive to the presence of photoexcited charges generated in the adjacent layers above and/or below the SLG.[14] Hence it provides a suitable platform for studies of photoexcited charge transfer.[14] Despite a growing number of experimental reports on the application of perovskite NC/graphene in optoelectronic devices,[8−10] one of the key challenges is understanding and controlling the charge transfer at the interface of these heterostructures.[15]

Here, we study the optoelectronic properties of graphene decorated with a layer of inorganic cesium lead halide nanocrystals ($CsPbX_3$, where X = Br or I). These hybrid devices have electrical and optical properties significantly different from those of pristine graphene or those decorated with traditional colloidal semiconductor nanocrystals. Our experimental data and modeling indicate that the optoelectronic properties of these devices are defined by the presence of deep trap energy levels ($E_x \approx 0.3$ eV) in the perovskite NCs. These NCs are responsible for large gate-voltage-induced

Received: October 11, 2019
Accepted: December 10, 2019
Published: December 10, 2019

DOI: 10.1021/acsaelm.9b00664
ACS Appl. Electron. Mater. 2020, 2, 147−154

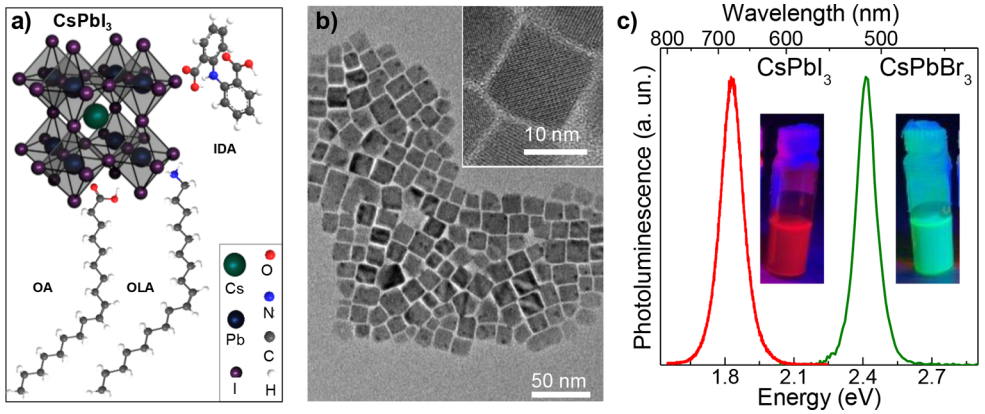

Figure 1. (a) A schematic diagram of the unit cell of $CsPbI_3$ nanocrystals capped with a mixture of oleic acid (OA), oleylamine (OLA), and iminodiacetic acid (IDA). (b) Representative TEM and HR TEM images of $CsPbI_3$ nanocrystals. (c) PL spectra and images of $CsPbBr_3$, and $CsPbI_3$ perovskites excited by unfocused UV light (365 nm).

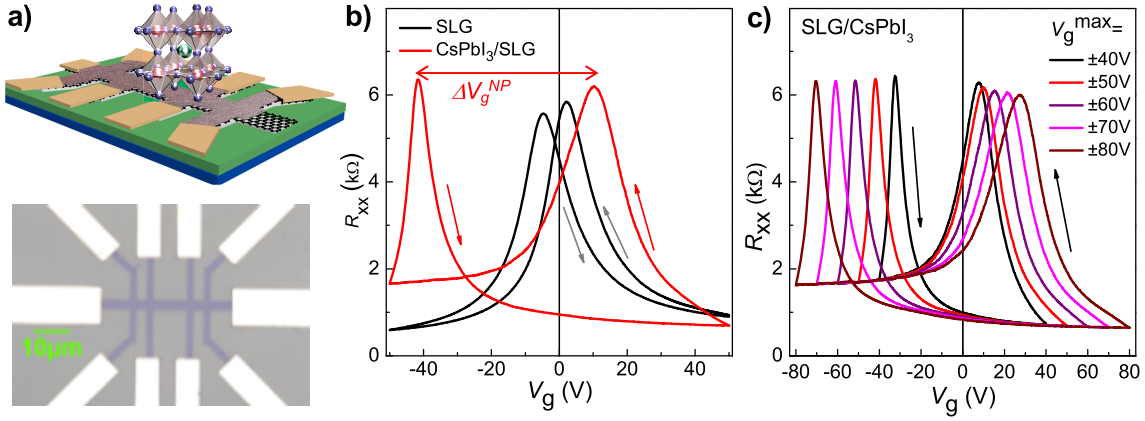

Figure 2. (a) A schematic diagram of the layer structure (top) and optical microscope image (bottom) of the Si/SiO_2/hBN/graphene/perovskite Hall bar device. (b) Room temperature dependence of the longitudinal resistance, R_{xx}, on applied gate voltage, V_g, of a pristine graphene device and of the same device after deposition of the $CsPbI_3$ nanocrystals. Arrows indicate directions of the V_g sweeps, sweep rate = 0.3 V/sec, T = 295 K. The top horizontal arrow represents the size of the ΔV_g^{NP}. (c) R_{xx} as a function of the maximum applied gate voltage, V_g^{max}, for a series of sequential V_g sweeps with V_g^{max} increasing from 40 to 80 V, sweep rate = 0.3 V/sec, T = 295 K.

hysteresis of the resistance and high photoresponsivity of these hybrid devices. A mechanism for this large hysteresis is proposed here. The high photoresponsivity ($R \approx 10^7$ A/W) in the UV−vis (250 nm to ~700 nm) arises from a large internal gain due to efficient transfer of photogenerated electrons from the NCs to SLG and a long lifetime (~1 s) of photoexcited holes that are trapped in the NCs. Our results offer a novel route for engineering the interface properties of hybrid materials, relevant for their exploitation in silicon-compatible optoelectronics.

RESULTS AND DISCUSSION

1. Electrical Properties of Perovskite Decorated Graphene Transistors. Cesium lead halide perovskite nanocrystals were synthesized following the method reported in ref 16 and were capped with a mixture of oleic acid (OA), oleylamine (OLA), and iminodiacetic acid (IDA) (Figure 1a). The nanocrystals have cubic shape with an average size of 12.9 ± 1.7 nm (Figure 1b). The composition of the NCs is chosen to tune their optical properties: $CsPbI_3$ and $CsPbBr_3$ NCs emit light at wavelengths of λ = 680 and 515 nm, respectively (Figure 1c). The NCs were deposited onto CVD-grown graphene by drop casting. The single layer graphene (SLG) was placed on a $hBN/SiO_2/Si$ substrate (SiO_2 layer thickness 285 nm; monolayer of hBN). The structures were then processed into two device geometries: Hall bars for measurements of carrier concentration and mobility (Figure 2a) and two-terminal diodes with short (~5 μm) channels for optoelectronic characterization.

We now compare the gate voltage characteristics of devices based on pristine graphene and perovskite-decorated graphene. The pristine SLG devices have a resistance maximum $R_{xx} \approx 6$ kΩ close to V_g = 0 V and exhibit only a small hysteresis loop, which we quantify in terms of the difference in the gate voltage value at charge neutrality (Dirac) point, ΔV_g^{NP} = 5 V, between the forward (from negative to positive bias) and reverse sweeps of V_g (Figure 2b and Supporting Information section SI1). The pristine SLG devices have a low electron carrier concentration of $n \approx 2 \times 10^{11}$ cm^{-2} at V_g = 0 V and carrier mobility $\mu_e \approx$ 6000 cm^2 V^{-1} s^{-1} at room temperature.

Deposition of the perovskite NCs leads to a significant increase of the hysteresis of the graphene charge neutrality point V_g^{NP}, that is, the gate voltage at which $R_{xx}(V_g)$ reaches its maximum value. Our measurements confirm that a film of perovskite nanocrystals has resistance >10 GΩ, which is not affected by applied gate voltage and/or exposure to light (see Supporting Information, section SI2). As shown in Figure 2b for SLG/$CsPbI_3$, at room temperature a hysteresis of $V_g^{NP} \approx 60$

DOI: 10.1021/acsaelm.9b00664
ACS Appl. Electron. Mater. 2020, 2, 147−154

V is observed for a gate voltage sweep over the range of V_g^{max} = ±50 V. The hysteresis of $R_{xx}(V_g)$ is strongly affected by the maximum applied gate voltage V_g^{max} (Figure 2c). The value of the hysteresis, ΔV_g^{NP}, increases with increasing V_g^{max} and reaches unexpectedly high values above 100 V. The observed dependence of the ΔV_g^{NP} on V_g^{max} and the large hysteresis indicate that the NC layer is accumulating a significant amount of charge. Due to the large hysteresis, it is not possible to define an exact value of the V_g^{NP} for the perovskite decorated layer; hence change of carrier concentration in the SLG due to surface doping effect of the perovskite NCs cannot be assessed quantitatively. We note that the hysteresis is reproducible and the overall device performance is fully reversible (Supporting Information, section SI3).

The observed ΔV_g^{NP} hysteresis is strongly temperature-dependent (Figure 3a). The $R_{xx}(V_g)$ of SLG/$CsPbI_3$ Hall bar

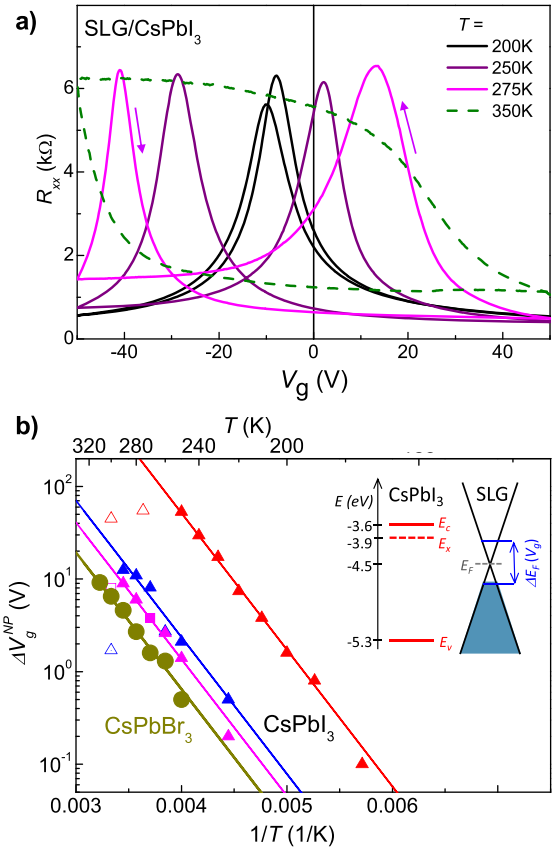

Figure 3. (a) $R_{xx}(V_g)$ dependences of the SLG/$CsPbI_3$ device measured at different temperatures. (b) Data points: ΔV_g^{NP} as a function of temperature for a Hall bar $CsPbI_3$/SLG device (red triangles) and three 2-terminal devices: two $CsPbI_3$/SLG devices (blue and magenta triangles) and one $CsPbBr_3$/SLG device (yellow circles). Solid lines represent a fit with $\Delta V_g^{NP} \approx \exp(-E_x/kT)$ with E_x = 0.3 eV. Inset: Band diagram of the $CsPbI_3$/SLG heterostructure. The blue arrow indicates a region where graphene Fermi energy, E_F, is changed by the applied gate voltage. The red dashed line denoted with E_x represents the energy level of charge trapping defects.

devices were measured over the range of temperatures from 2 to 350 K. The size of the hysteresis decreases with decreasing temperature and quenches at $T \approx 200$ K, where the observed $R_{xx}(V_g)$ characteristics resemble those of pristine graphene, indicating that no charge transfer is taking place at $T < 200$ K. At $T > 320$ K, a significant broadening of the forward/reverse loop is observed. This is likely due to structural changes in the perovskite NCs, which is also evident in the irreversible decrease of room temperature photoluminescence (PL) intensity following exposure of the NCs to $T > 400$ K. We note that the room temperature optical properties of the NCs, such as PL, are not significantly affected by exposure to temperatures in the range from 2 K < T < 400 K. This leads us to conclude that the dramatic $\Delta V_g^{NP}(T)$ dependence is related to the charge transfer between the NC layer and the SLG, rather than the temperature-dependent properties of the perovskite NCs.

The temperature dependence of the ΔV_g^{NP} hysteresis between 200 K < T < 300 K has an exponential form and is well described by $\Delta V \approx \exp(-E_x/kT)$, with activation energy of E_x = 0.3 eV. This activation energy has the same value for both $CsPbI_3$ and $CsPbBr_3$ NCs (Figure 3b), suggesting the presence of a common deep energy level defect (inset Figure 3b). We note that the activation energy is significantly larger, E_x = 0.6 eV, for $Cs(Pb_{0.67}Sn_{0.33})I_3$ NCs (see Supporting Information section SI3). Thus, we infer that these defect energy levels correspond to Pb-related defects, which were recently reported to account for PL intermittency in cesium lead halide nanocrystals.[17] In order to understand the nature of the ΔV_g^{NP} hysteresis, we consider a numerical two capacitor (2C) model, described below.

2. Modeling of Charge Transfer in Perovskite Decorated SLG. The small hysteresis of $R_{xx}(V_g)$ is typically observed in gated SLG devices and usually associated with the gate capacitance and/or charging of impurities.[18,19] In pristine SLG devices, the amount of hysteresis is very small (Figure 2b) and is independent of the V_g sweep range (V_g^{max}). In perovskite-decorated SLG we observe an anomalously large hysteresis, ΔV_g^{NP}, which is not observed in other hybrid graphene heterostructures.[6,7,23] We envisage that the slow V_g-dependent charge transfer between the NCs and SLG results from charge accumulation in the NC layer.

In our numerical model, we treat our $CsPbI_3$/SLG/SiO_2/Si device as a double capacitor (2C-model): the first capacitor is that of the gate/SiO_2/SLG layers and the second capacitor is the "effective" capacitance of a layer of perovskite nanocrystals (see inset in Figure 4b and Figure S5). The resistance of the NC layer is very high (>10 GΩ; see Figure S2), hence, the charge transfer between the neighboring NCs is negligibly small. In this model we consider charge transfer only from the layer of NCs adjacent to the SLG; the only fitting parameter is the time constant, τ_{per}, which describes the rate at which the charge in the perovskites decays.

Our numerical calculations of the $R_{xx}(V_g)$ hysteresis at different V_g^{max} (Figure 4a) demonstrate a behavior similar to that observed experimentally (Figure 2c). By fitting the measured $\Delta V_g^{NP}(V_g^{max})$ dependences by means of the 2C model (Figure 4b) we obtain a good agreement between the experimental data and numerical simulations with a value of the fitting parameter τ_{per} = 130 s. However, the symmetric behavior with respect to positive/negative V_g predicted by this model is not consistent with the measured data. The experimental results (Figure 2c) reveal a weaker hysteresis at positive V_g. We attribute this discrepancy to the assumption used in our model we disregard which capacitor plate, bottom gate, or top SLG with NCs plate, has positive/negative polarity. In our device, the charging of the top plate of the capacitor (SLG with NCs) depends on the polarity of the applied gate voltage as it shifts the Fermi energy in the SLG,

DOI: 10.1021/acsaelm.9b00664
ACS Appl. Electron. Mater. 2020, 2, 147−154

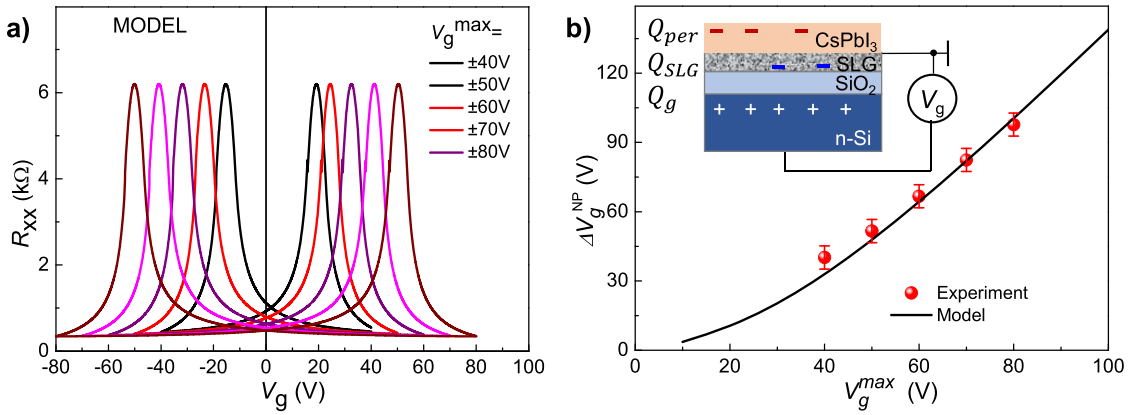

Figure 4. (a) Numerical simulation using 2C-model of $R_{xx}(V_g)$ with increasing V_g^{max}. The fitting parameter used is τ_{per} = 130 s. (b) Data points represent measured values of ΔV_g^{NP} as a function of the V_g^{max} (see Figure 2c). The solid line is a fit based on the two-capacitor 2C-model with τ_{per} = 130 s. The inset shows schematically the distribution of charge between the perovskite layer, Q_{per}, the graphene layer, Q_{SLG}, and the gate, Q_g, used in the 2C-model.

over the range ±0.3 eV for ±100 V (Supporting Information section SI4).

The gate voltage sweep generates an incremental increase in charge $\Delta Q = C\Delta V_g$ on the top of the perovskite/SLG electrode corresponding to the sum of free carrier charge (electrons or holes) in the SLG and the charge bound to the localized states of the NCs, with activation energy, E_x. We assume that most of this charge is stored in the NC layer and is slowly released into the SLG (with an effective time constant of ~100 s). The charge capacitance of the perovskite NC layer is estimated from the measured position of the SLG neutrality point hysteresis, $\Delta V_g^{NP} > 100$ V, to be greater than 7×10^{12} cm^{-2} (see Figure 2c). Assuming that the average size of our $CsPbI_3$ NCs with ligands included is $a \approx 15$ nm[16] and the surface filling factor is approximately 1, we estimate the NC density to be approximately 4×10^{11} cm^{-2}. Hence the number of individual charges per single NC adjacent to the SLG is greater than 10. We estimate that a perovskite nanocrystal contains ~400 of $CsPbX_3$ unit cells, each containing a single Pb atom, per one side of a NC cube, thus providing an extremely large maximum charge capacity, limited only by Coulomb repulsion of the charges within the perovskite NC. The electrostatic energy which arises when $N = 10$ electrons are accommodated within a single perovskite NC can be estimated using the expression $U = \frac{3}{5}\frac{e^2N^2}{4\pi\varepsilon\varepsilon_0 a}$, where $a = 7$ nm is an effective radius of a NC and $\varepsilon = 10$ is the dielectric constant of $CsPbI_3$.[20] The estimated value is $U \approx 0.6$ eV, which is significantly lower than the $CsPbI_3$ work function of ~3.6 eV.[21]

We propose that the large number of charges trapped within a single perovskite NC is responsible for the anomalously large ΔV_g^{NP} hysteresis and slow charge transfer processes. Indeed, our model is in good agreement with the observed dependence of hysteresis ΔV_g^{NP} on the applied gate voltage (Figure 4b). A similar charge transfer between SLG and an adjacent dielectric layer was recently reported in SiC/SLG[22] and in InSe/graphene[23,24] heterostructures. In both heterostructures, the Fermi level in SLG is pinned to the energy level of the ionized donor impurities in the adjacent SiC or InSe dielectric layer. However, in contrast to our perovskite-decorated devices, no large temperature- and V_g sweep range- dependence of the pinning effect was reported for those devices.[22−24] This suggests that charge transfer processes in our 0D/2D $CsPbI_3$/SLG hybrid devices are significantly slower than those in 2D/2D heterostructures.

3. Light-Induced Charge Transfer and Photoresponsivity. The charge transfer is affected by exposure to light. We observed a significant reduction of the hysteresis under positive gate voltage and under light illumination, with V_g^{NP} always remaining in the negative V_g region. In addition, the negative V_g section of the $R_{xx}(V_g)$ curves is similar for both light and dark conditions (inset in Figure 5a). This behaviour can be explained by the effect of light on the gate-induced charge trapped in the perovskite NCs. The light generates electron−hole pairs in the NCs and the photoexcited electrons are quickly transferred to the SLG, while the less mobile photoexcited holes remain trapped in the NCs. This difference in relaxation times of photoexcited electrons and holes leads to the asymmetry of the $R_{xx}(V_g)$ shown in Figure 5a. We assume that photoexcited holes can recombine with gate-induced negative charges in the perovskite NCs (Figure 5b). The V_g-dependence of the resistance indicates the transfer of both photoexcited electrons and holes for $V_g > 0$ V, and the preferential transfer of photoexcited electrons for $V_g < 0$ V (see corresponding band diagrams in Figure 5b and in Figure S8). Our macroscopic capacitance model accounts well for these experimental findings. This process can be described in terms of a significant reduction of the τ_{per} parameter under illumination and at applied positive V_g. Under negative V_g conditions, photoexcited holes do not interact with positive gate-induced charge, leading to no significant changes in the $R_{xx}(V_g)$ hysteresis measured under dark and light conditions (section SI5).

The shift of V_g^{NP} toward negative values under light illumination (Figure 5a) indicates a transfer of photoexcited electrons from the perovskite NCs to the graphene (Figure 5b), similar to that reported previously for quantum dot decorated SLG[4,5,25] and other perovskite NC decorated structures.[10] This behavior is in contrast to the transfer of photoexcited holes suggested for mixed-cation lead mixed-halide hybrid perovskite deposited on similar CVD graphene/SiO_2/Si substrates.[15]

The SLG/perovskite devices are photosensitive over the wavelength range of optical absorption of the NCs. The photocurrent spectrum is quite similar to that of optical absorption (Supporting Information SI5): it follows quite

DOI: 10.1021/acsaelm.9b00664
ACS Appl. Electron. Mater. 2020, 2, 147−154

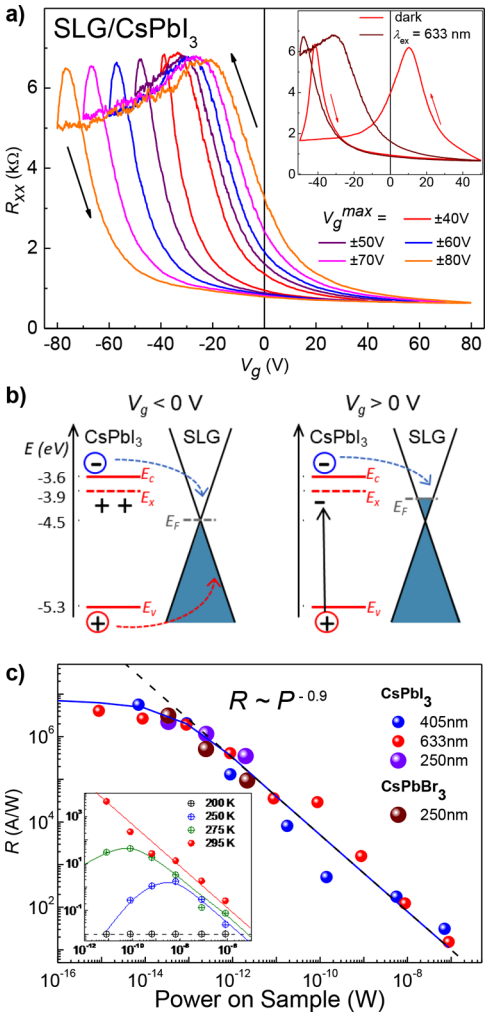

Figure 5. (a) R_{xx} as a function of the maximum applied gate voltage, V_g^{max}, for a series of sequential V_g sweeps with V_g^{max} increasing from 40 to 80 V, under excitation with a HeNe laser (λ = 633 nm, P = 310 W/m^2. Inset: V_g^{max} = ±50 V sweep in the dark and under laser light. (b) A schematic diagram of the $CsPbI_3$/SLG band structure. Arrows indicate transfer of photoexcited charges from perovskites to the SLG (dashed blues and red arrows) for negative (left) and positive (right) gate voltages. The vertical black arrow indicates recombination of photogenerated holes with negative charge stored in the perovskite layer. (c) UV−vis photoresponsivity of $CsPbI_3$/SLG and $CsPbBr_3$/SLG devices excited at λ = 633, 405, and 250 nm. The dashed line is a fit using $R \approx P^{-0.9}$. The blue line is a guide to the eye. Inset: photoresponsivity of $CsPbI_3$/SLG at different temperatures measured at 10^{-11} W < P < 10^{-6} W region. The dashed line represents the level of noise.

closely that of absorbance. Also, a large photocurrent is observed in the UV region (<400 nm). Pristine graphene has a small optical absorbance (~2%) and consequently its photoresponsivity is very low (<0.1 A/W). Hence, the optical response of these SLG/perovskites heterostructures is determined mainly by the optical absorption of the perovskite NCs and by the charge transfer between the NC layer and graphene. The SLG devices decorated with both types of perovskite NCs, $CsPbBr_3$, and $CsPbI_3$, have very high photoresponsivity of $R > 10^6$ A/W in the UV−vis range (250 nm −633 nm) at room temperature (Figure 5c). The highest responsivity $R \approx 5 \times 10^6$ A/W is observed in the low power limit where the noise equivalent power NEP ≈ 10^{-15} W. The responsivity exceeds that recently reported for SLG devices decorated with similar perovskite nanocrystals.[9,26] In particular, we note the higher responsivity of our devices in the UV range. With increasing excitation power, the photoresponsivity decreases as $R \sim P^{-x}$, where x = 0.90 ± 0.02 (Figure 5c), which is similar to that reported for $CsPbCl_3$[9] and for colloidal quantum dots.[5]

We now examine the temperature dependence of the power law as $R \sim P^{-x}$ at power on the sample above 10^{-11} W. As can be seen in the inset in Figure 5c, with decreasing temperature we observe a deviation from the power law. For example, at T = 250 K, the power dependence of the responsivity is described by $R \sim P^{-0.9}$ only up to the value of $P = 10^{-9}$ W. At T = 200 K, the responsivity decreases, reaching a value of R < 1 A/W, which is similar to that of pristine graphene. This observation corroborates our measurements of the temperature dependence of the gate voltage-induced hysteresis ΔV_g^{NP}, where at T < 200 K, no effect of the NC layer on the electrical properties of graphene is observed (Figure 3a). We attribute the observed temperature dependence of $R(P)$ to the interplay of two opposing effects: the $R \sim P^{-0.9}$ increase of $R(P)$ at the high power range and the fast exponential quench of $R(T)$ at low P. The weaker $R(T)$ dependence at large excitation power can be explained by the heating of the device. At low excitation powers ($P < 10^{-8}$ W) and low temperatures (T < 250 K) charge transfer between the NCs and graphene appears to be blocked. This results in quenching of both the photoresponsivity R and the gate voltage hysteresis ΔV_g^{NP}. There is only significant change of the NC/SLG properties that are directly dependent on the NC-SLG charge transfer, such as the NC photoluminescence[27] or the SLG carrier concentration and mobility over a wide temperature range.

4. Temporal Response of Perovskite/SLG Devices. The temporal response of the devices was measured at room temperature to explore the possible mechanisms underlying charge transfer and device performance. A reproducible response to optical excitation is observed for all samples with ON/OFF response times of ~2 s (Figure 6a). The temporal relaxation of the photocurrent cannot be fitted to a single exponential dependence, indicating the presence of several processes responsible for charge relaxation in these heterostructures, with characteristic times in the range from 0.5 to 5 s. The studies of temporal relaxation following electrical excitation by the applied gate voltage revealed a longer characteristic relaxation time of ~120 s (Figure 6b). Note that this time is very close to the τ_{per} parameter used in our 2C-model to fit the $\Delta V_g^{NP}(V_g^{max})$ data (Figure 4b).

The temporal response of the device following optical excitation is shown in Figure 6a. The observed exponential decay of the resistance has characteristic times of ~1 s. The relaxation of the charge generated by applied gate voltage has a significantly slower decay time of ~100 s (Figure 6b). We ascribe this difference to the relaxation of fast optically excited, high energy charge carriers compared to slow gate-voltage-induced charge transfer. Despite significant differences in the values of the relaxation times, the optical responsivity R and gate voltage hysteresis ΔV_g^{NP} have very similar temperature dependences (Figure 6c). This leads us to conclude that the processes responsible for the ΔV_g^{NP} hysteresis also define the optical responsivity observed in these materials, that is, both light- and gate-induced charge trapping processes are controlled by the same kind of charge traps with an activation energy $E_x \approx 0.3$ eV.

DOI: 10.1021/acsaelm.9b00664
ACS Appl. Electron. Mater. 2020, 2, 147−154

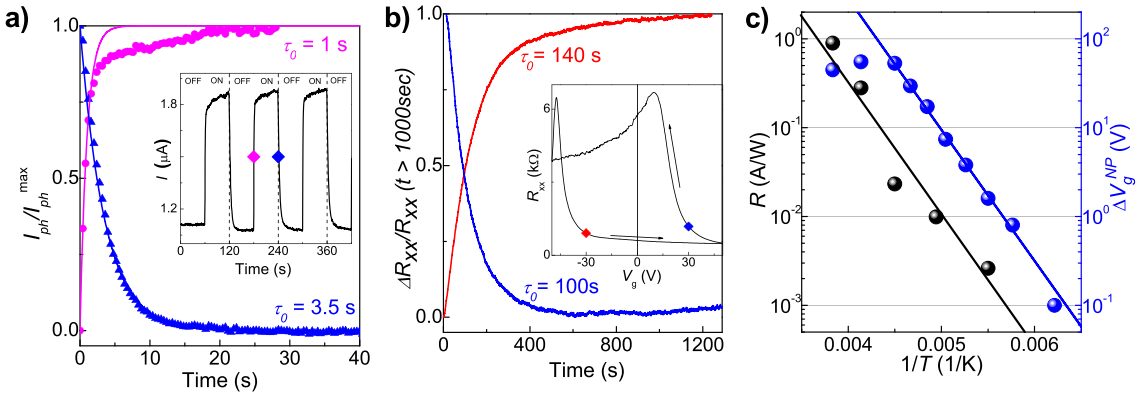

Figure 6. (a) Temporal response of the photocurrent on rising and falling slope (ON/OFF) at point indicated by magenta (ON) and blue (OFF) points in the inset for the SLG/$CsPbI_3$ device. Inset: light on/off time dependence of the photocurrent for the SLG/$CsPbI_3$ device at T = 295 K (V_{sd} = 20 mV, V_g = 0 V, P = 325 W/m^2, λ = 633 nm). (b) Temporal response and (inset) R_{xx} as a function of V_g for $CsPbI_3$ /SLG device at the V_g-sweep positions indicated by the red and blue dots (inset), T = 295 K, I_{sd} = 0.5 μA, sweep rate 0.3 V/sec. (c) Data points: $\Delta V_g^{NP}(T)$ (blue) and $R(T)$ (black) dependences of SLG/$CsPbI_3$ device. Solid lines are the fit with $\Delta V \approx \exp(-E_x/kT)$, where E_x = 0.3 eV.

The response time of these devices is independent of temperature. However, at low temperatures (T < 270 K) the perovskites/SLG photodetectors become less stable, introducing telegraph noise and an unstable photoresponse. The relatively large ratio of the lifetime of the photoexcited holes trapped in the NCs, typically τ_{NC} > 1 s and the electron transit time in graphene channel, τ_e < 1 ns, give rise to high photoresponsivity (R > 10^6 A/W at T = 295 K) due to high photogain.[5,9] The measured response time of ~1 s in our devices (Figure 6a) is comparable to that previously reported for QD-decorated graphene photodetectors[4,5] and is significantly shorter than that of $CsPbCl_3$/graphene devices without ligand treatment (>100 s[9]). We propose that the shorter ligands used in our NCs (IDA replacement) enable more efficient charge transfer between the NC layer and the SLG, and hence shorter response times.

CONCLUSIONS

We have described how inorganic perovskite ($CsPbX_3$) nanocrystals can be been used as a photosensitive layer in $CsPbX_3$/graphene planar photon detectors. These detectors have stable performance and record high (>10^6 A/W) photoresponsivity in the UV−vis (250−633 nm) range. The $CsPbX_3$ NC decorated graphene devices exhibit an anomalous charging effect resulting in a large (>100 V) hysteresis in the gate voltage dependence of the resistance, $R_{xx}(V_g)$. The temperature dependence of the optoelectronic and transport properties of these devices has been studied for the first time and reveals fast quenching of the device performance in the temperature range below ambient conditions (T = 200−300 K). This phenomenon is consistent with the presence of a deep (~0.3 eV) defect level in all $CsPbX_3$ perovskites which we have investigated. The precise nature of this defect level is unknown and requires further studies, but is likely to be associated with the Pb atoms. These $CsPbX_3$/graphene devices offer good prospects for the development of ultrasensitive 0D/2D UV photon detectors.

MATERIALS AND METHODS

Synthesis and Characterization of Perovskite NCs. We have synthesized cesium lead halide $CsPbX_3$ perovskite NCs with improved properties by postsynthesis replacement of oleic acid ligands with iminodibenzoic acid: the NCs have a long shelf life in solution (>2 months), are stable under different environmental conditions, and have a high quantum yield of up to 90% in the visible spectral range.[16] Two different perovskites, $CsPbI_3$ and $CsPbBr_3$, have been tested in order to optimize device stability, and maximize optical absorption and photoresponse in the UV range.

Device Fabrication. In these devices we utilized commercial CVD monolayer graphene/CVD monolayer hBN heterostructures on 285 nm SiO_2/Si substrates purchased from Graphene Supermarket. The 0D/2D devices were fabricated using a combination of electron beam lithography and liquid deposition of nanocrystals (NCs) in two different planar geometries: a multiterminal Hall bar and a planar diode with a short channel length. The Hall bar geometry is used for magneto-transport measurements, enabling the precise measurement of carrier concentration and mobility (Hall effect and 4-terminal conductivity measurements). The short two-terminal diodes are used for measurements of photocurrent and photoresponsivity with a short electron transit time and reduced edge effects due to a smaller number of carrier traps at the edges of 2D layers.

Electrical and Optical Measurements. Electrical measurements of the $R_{xx}(V_g)$ and photocurrent measurements vs light power or time were performed in the DC mode using Keithley-2400 source-meters and Keitheley-2010 multimeters. Wavelength dependent measurements of the photocurrent and photoresponsivity were performed using the lock-in technique with the light passed through a monochromator modulated by a chopper with a frequency of 17 Hz. For the fixed wavelength excitation, we used a HeNe laser (633 nm) or solid-state lasers (405 and 532 nm). A deuterium lamp equipped with a short-pass filter was used as a UV (250 nm) source. Photoluminescence studies were conducted using a Horiba Jobyn Yvon micro-PL system, equipped with a frequency-doubled Nd:YVO4 laser (λ = 532 nm), HeNe laser (λ = 633 nm), and Si charge-coupled device (CCD) camera. The optical absorption spectra were measured using an Edinburgh Instruments FLS980 fluorescence spectrometer equipped with an integrating sphere module.

ASSOCIATED CONTENT

Supporting Information

The Supporting Information is available free of charge at https://pubs.acs.org/doi/10.1021/acsaelm.9b00664.

Description of the properties of pristine graphene devices and additional data on temperature dependence of the hysteresis; detailed description of the numerical modeling of charging effect in the perovskite/SLG; and additional data for the photosensitivity of the SLG/perovskite devices (PDF)

DOI: 10.1021/acsaelm.9b00664
ACS Appl. Electron. Mater. 2020, 2, 147−154

AUTHOR INFORMATION

Corresponding Author

*E-mail: Lyudmila.Turyanska@nottingham.ac.uk.

ORCID

Lyudmila Turyanska: 0000-0002-9552-6501

Notes

The authors declare no competing financial interest.

ACKNOWLEDGMENTS

This work was supported by the Defence Science and Technology Laboratory (DSTL); the Engineering and Physical Sciences Research Council [Grant Nos. EP/K503800/1]; and the Faculty of Science, University of Nottingham. We thank the University of Nottingham Propulsion Futures Beacon for funding towards this research. E.E.V. acknowledges support from the Russian Science Foundation (17-12-01393). We acknowledge access to the facilities provided by the Nanoscale and Microscale Research Centre (nmRC) and Dr Michael W. Fay with transmission electron microscopy. We also benefit from useful discussions with colleagues from the DSTL.

REFERENCES

(1) Koppens, F. H. L.; Mueller, T.; Avouris, Ph.; Ferrari, A. C.; Vitiello, M. S.; Polini, M. Photodetectors Based on Graphene, Other Two-Dimensional Materials and Hybrid Systems. *Nat. Nanotechnol.* **2014**, *9*, 780−793.

(2) De Sanctis, A.; Mehew, J. D.; Craciun, M. F.; Russo, S. Graphene-Based Light Sensing: Fabrication, Characterisation, Physical Properties and Performance. *Materials* **2018**, *11*, 1762.

(3) Liu, Y.; Zhang, S.; He, J.; Wang, Z. M.; Liu, Z. Recent Progress in the Fabrication, Properties, and Devices of Heterostructures Based on 2D Materials. *Nano-Micro Lett.* **2019**, *11*, 13.

(4) Ferrari, A. C.; Bonaccorso, F.; Fal'ko, V.; Novoselov, K. S.; Roche, S.; Bøggild, P.; Borini, S.; Koppens, F. H. L.; Palermo, V.; Pugno, N.; Garrido, J. A.; Sordan, R.; Bianco, A.; Ballerini, L.; Prato, M.; Lidorikis, E.; Kivioja, J.; Marinelli, C.; Ryhänen, T.; Morpurgo, A.; Coleman, J. N.; Nicolosi, V.; Colombo, L.; Fert, A.; Garcia-Hernandez, M.; Bachtold, A.; Schneider, G. F.; Guinea, F.; Dekker, C.; Barbone, M.; Sun, Z.; Galiotis, C.; Grigorenko, A. N.; Konstantatos, G.; Kis, A.; Katsnelson, M.; Vandersypen, L.; Loiseau, A.; Morandi, V.; Neumaier, D.; Treossi, E.; Pellegrini, V.; Polini, M.; Tredicucci, A.; Williams, G. M.; Hee Hong, B.; Ahn, J.-H.; Kim, J. M.; Zirath, H.; van Wees, B. J.; van der Zant, H.; Occhipinti, L.; Di Matteo, A.; Kinloch, I. A.; Seyller, T.; Quesnel, E.; Feng, X.; Teo, K.; Rupesinghe, N.; Hakonen, P.; Neil, S. R. T.; Tannock, Q.; Löfwander, T.; Kinaret, J. Science and Technology Roadmap for Graphene, Related Two-Dimensional Crystals, and Hybrid Systems. *Nanoscale* **2015**, *7*, 4598−5062.

(5) Turyanska, L.; Makarovsky, O.; Svatek, S. A.; Beton, P. H.; Mellor, C. J.; Patanè, A.; Eaves, L.; Thomas, N. R.; Fay, M. W.; Marsden, A. J.; Wilson, N. R. Ligand-Induced Control of Photoconductive Gain and Doping in a Hybrid Graphene−Quantum Dot Transistor. *Adv. Electron. Mater.* **2015**, *1*, 1500062.

(6) Cheng, J.; Wang, C.; Zou, X.; Liao, L. Recent Advances in Optoelectronic Devices Based on 2D Materials and Their Heterostructures. *Adv. Opt. Mater.* **2019**, *7*, 1800441.

(7) Goossens, S.; Navickaite, G.; Monasterio, C.; Gupta, S.; Piqueras, J. J.; Pérez, R.; Burwell, G.; Nikitskiy, I.; Lasanta, T.; Galán, T.; Puma, E.; Centeno, A.; Pesquera, A.; Zurutuza, A.; Konstantatos, G.; Koppens, F. Broadband image sensor array based on graphene−CMOS integration. *Nat. Photonics* **2017**, *11*, 366−371.

(8) Lee, Y.; Kwon, J.; Hwang, E.; Ra, C.-H.; Yoo, W. J.; Ahn, J.-H.; Park, J. H.; Cho, J. H. High-Performance Perovskite−Graphene Hybrid Photodetector. *Adv. Mater.* **2015**, *27*, 41−46.

(9) Gong, M.; Sakidja, R.; Goul, R.; Ewing, D.; Casper, M.; Stramel, A.; Elliot, A.; Wu, J. Z. High-Performance All-Inorganic $CsPbCl_3$ Perovskite Nanocrystal Photodetectors with Superior Stability. *ACS Nano* **2019**, *13*, 1772−1783.

(10) Miao, J.; Zhang, F. Recent Progress on Highly Sensitive Perovskite Photodetectors. *J. Mater. Chem. C* **2019**, *7*, 1741.

(11) Mei, F.; Sun, D.; Mei, S.; Feng, J.; Zhou, Y.; Xu, J.; Xiao, X. Recent Progress in Perovskite-Based Photodetectors: The Design of Materials and Structures. *Advances in Physics: X* **2019**, *4*, 1592709.

(12) Al Amri, A. M.; Leung, S.-F.; Vaseem, M.; Shamim, A.; He, J.-H. Fully Inkjet-Printed Photodetector Using a Graphene/Perovskite/Graphene Heterostructure. *IEEE Trans. Electron Devices* **2019**, *66*, 2657−2661.

(13) Fang, C.; Wang, H.; Shen, Z.; Shen, H.; Wang, S.; Ma, J.; Wang, J.; Luo, H.; Li, D. High-Performance Photodetectors Based on Lead-Free 2D Ruddlesden−Popper Perovskite/MoS2 Heterostructures. *ACS Appl. Mater. Interfaces* **2019**, *11*, 8419−8427.

(14) Georgakilas, V.; Otyepka, M.; Bourlinos, A. B.; Chandra, V.; Kim, N.; Kemp, K. C.; Hobza, P.; Zboril, R.; Kim, K. S. Functionalization of Graphene: Covalent and Non-Covalent Approaches, Derivatives and Applications. *Chem. Rev.* **2012**, *112*, 6156−6214.

(15) Brus, V. V.; Lang, F.; Fengler, S.; Dittrich, T.; Rappich, J.; Nickel, N. H. Doping Effects and Charge-Transfer Dynamics at Hybrid Perovskite/Graphene Interfaces. *Adv. Mater. Interfaces* **2018**, *5*, 1800826.

(16) Zhang, C.; Turyanska, L.; Cao, H.; Zhao, L.; Fay, M. W.; Temperton, R.; O'Shea, J.; Thomas, N. R.; Wang, K.; Luan, W.; Patanè, A. Hybrid light emitting diodes based on stable, high brightness all-inorganic CsPbI3 perovskite nanocrystals and InGaN. *Nanoscale* **2019**, *11*, 13450−13457.

(17) Hou, L.; Zhao, C.; Yuan, X.; Zhao, J.; Krieg, F.; Tamarat, P.; Kovalenko, M. V.; Guo, C.; Lounis, B. Memories in the Photoluminescence Intermittency of Single Cesium Lead Bromide Nanocrystals. arXiv.org/physics/arXiv:1909.03378. e-print.https://arxiv.org/ftp/arxiv/papers/1909/1909.03378.pdf.

(18) Wang, H.; Wu, Y.; Cong, C.; Shang, J.; Yu, T. Hysteresis of Electronic Transport in Graphene Transistors. *ACS Nano* **2010**, *4*, 7221−7228.

(19) Mohrmann, J.; Watanabe, K.; Taniguchi, T.; Danneau, R. Persistent Hysteresis in Graphene-Mica van der Waals Heterostructures. *Nanotechnology* **2015**, *26*, 015202.

(20) Yang, Z.; Surrente, A.; Galkowski, K.; Miyata, A.; Portugall, O.; Sutton, R. J.; Haghighirad, A. A.; Snaith, H. J.; Maude, D. K.; Plochocka, P.; Nicholas, R. J. Impact of the Halide Cage on the Electronic Properties of Fully Inorganic Cesium Lead Halide Perovskites. *ACS Energy Lett.* **2017**, *2*, 1621−1627.

(21) Zhang, T.; Wu, J.; Zhang, P.; Ahmad, W.; Wang, Y.; Alqahtani, M.; Chen, H.; Gao, C.; Chen, J. D.; Wang, Z.; Li, S. High Speed and Stable Solution-Processed Triple Cation Perovskite Photodetectors. *Adv. Opt. Mater.* **2018**, *6*, 1701341.

(22) Alexander-Webber, J. A.; Huang, J.; Maude, D. K.; Janssen, T. J. B. M.; Tzalenchuk, A.; Antonov, V.; Yager, T.; Lara-Avila, S.; Kubatkin, S.; Yakimova, R.; Nicholas, R. J. Giant Quantum Hall Plateaus Generated by Charge Transfer in Epitaxial Graphene. *Sci. Rep.* **2016**, *6*, 30296.

(23) Kudrynskyi, Z. R.; Bhuiyan, M. A.; Makarovsky, O.; Greener, J. D. G.; Vdovin, E. E.; Kovalyuk, Z. D.; Cao, Y.; Mishchenko, A.; Novoselov, K. S.; Beton, P. H.; Eaves, L.; Patanè, A. Giant Quantum Hall Plateau in Graphene Coupled to an InSe van der Waals Crystal. *Phys. Rev. Lett.* **2017**, *119*, 157701.

(24) Bhuiyan, M.; Kudrynskyi, Z. R.; Mazumder, D.; Greener, J. D. G.; Makarovsky, O.; Mellor, C. J.; Vdovin, E. E.; Piot, B. A.; Lobanova, I. I.; Kovalyuk, Z. D.; Nazarova, M.; Mishchenko, A.; Novoselov, K. S.; Cao, Y.; Eaves, L.; Yusa, G.; Patanè, A. Photoquantum Hall Effect and Light-Induced Charge Transfer at the Interface of Graphene/InSe Heterostructures. *Adv. Funct. Mater.* **2019**, *29*, 1805491.

(25) Turyanska, L.; Makarovsky, O.; Eaves, L.; Patane, A.; Mori, N. Mobility enhancement of CVD graphene by spatially correlated charges. *2D Mater.* **2017**, *4*, 025026.

DOI: 10.1021/acsaelm.9b00664
ACS Appl. Electron. Mater. 2020, 2, 147−154

(26) Surendran, A.; Yu, X.; Begum, R.; Tao, Y.; Wang, Y. J.; Leong, W. L. All Inorganic Mixed Halide Perovskite Nanocrystal−Graphene Hybrid Photodetector: From Ultrahigh Gain to Photostability. *ACS Appl. Mater. Interfaces* **2019**, *11*, 27064−27072.
(27) Diroll, B. T.; Nedelcu, G.; Kovalenko, M. V.; Schaller, R. D. High-Temperature Photoluminescence of $CsPbX_3$ (X = Cl, Br, I) Nanocrystals. *Adv. Funct. Mater.* **2017**, *27*, 1606750.

DOI: 10.1021/acsaelm.9b00664
ACS Appl. Electron. Mater. 2020, 2, 147−154